HAL open science

Dynamics of propagating front into sand ripples under regular waves

Julie Lebunetel-Levaslot, Armelle Jarno-Druaux, Alexander Ezersky, François Marin

To cite this version:

Julie Lebunetel-Levaslot, Armelle Jarno-Druaux, Alexander Ezersky, François Marin. Dynamics of propagating front into sand ripples under regular waves. Physical Review E : Statistical, Nonlinear, and Soft Matter Physics, 2010, 82 (3), 10.1103/PhysRevE.82.032301 . hal-02095110

HAL Id: hal-02095110

https://hal.science/hal-02095110v1

Submitted on 10 Apr 2019

HAL is a multi-disciplinary open access archive for the deposit and dissemination of scientific research documents, whether they are published or not. The documents may come from teaching and research institutions in France or abroad, or from public or private research centers.

L'archive ouverte pluridisciplinaire **HAL**, est destinée au dépôt et à la diffusion de documents scientifiques de niveau recherche, publiés ou non, émanant des établissements d'enseignement et de recherche français ou étrangers, des laboratoires publics ou privés.

PROOF COPY [ERJ1041] 168009PRE

Dynamics of propagating front into sand ripples under regular waves

J. Lebunetel-Levaslot,[1] A. Jarno-Druaux,[1] A. B. Ezersky,[2] and F. Marin[1,*]
[1]*Laboratoire Ondes et Milieux Complexes, FRE CNRS 3102, Université du Havre, 25 rue Philippe Lebon, BP 540, 76058 Le Havre Cedex, France*
[2]*Laboratoire Morphodynamique Continentale et Côtière, UMR CNRS 6143, Université de Caen, 2-4 rue des Tilleuls, 14000 Caen, France*
(Received 9 April 2010; revised manuscript received 20 July 2010)

The results of an experimental study of pattern formation on sandy bottom under the action of regular harmonic surface waves are reported. It is found that two modes of pattern formation occur: sand ripples form uniformly on the whole bottom or from localized nucleation sites. In the second regime, the ripples appear in isolated regions (patches) increasing in size, and front propagation speed is measured. A simple dynamical model based on the Ginzburg-Landau equation is proposed to explain the characteristics of patches.

DOI: XXXX PACS number(s): 45.70.Qj

I. INTRODUCTION

Pattern formation on a bottom under the action of surface waves has been investigated theoretically and experimentally for many years. The morphological characteristics of sand ripple patterns observed in the near shore region are important for the prediction of the dissipation of waves energy, and for the sediment transport. Ripples also influence the biological processes occurring on the bottom and the dispersion of pollutants. Ayrton [1] and Bagnold [2] carried out the pioneering works on these structures. Detailed investigations of the onset of instability caused by oscillating water over sand were performed in [3,4]. The formation of vortices at the lee side of the ripple crest and their ejection upward at flow reversal were considered in [5,6]. These vortices control the mass transfer between neighboring ripples during their formation [6,7], and the wavelength of fully developed ripples is proportional to the amplitude of the oscillatory flow [6,8]. The stability of bottom patterns in relation to changes of amplitude and frequency of water oscillations was studied in [9].

In this paper, we focus on the investigation of the amplification of initial perturbations of small amplitude leading to the formation of sand ripples. The front propagation plays a key role in the involved processes, and we present in this brief report a detailed investigation of the characteristics of this front. The study of front propagation has been considered in different unstable systems [10], and in particular in numerous hydrodynamic systems [11–13]. The phenomenon of front propagation for sand ripples under waves was mentioned in [2]. However, this propagation has not been accurately investigated to our knowledge. The aim of the present paper is to study the features of front propagation in sand ripple patterns. The main difference between sand ripples and the systems considered in [11–13] is the following. The action of regular surface waves (propagating usually in one direction) results in anisotropy of the sand ripples instability, and consequently of the front propagation velocity, whereas the systems studied in [11–13] may be considered as isotropic. The characteristics of fronts propagating in the same direction as surface waves or in the opposite direction are investigated in detail in the present study.

II. EXPERIMENTAL SETUP AND RESULTS

The experiments were performed in a 10 m long, 0.5 m high, and 0.49 m wide wave flume at Le Havre University. Regular surface waves were produced by an oscillating paddle at one end of the flume. At the other end a porous beach was installed to minimize wave reflection. The temporal evolution of the free surface was measured with two fixed resistive probes and analyzed with Goda's method [14]. The reflection coefficient was less than 5% for all of the tests. The mean water depth at rest was $d_*=27$ cm. Experiments were carried out in a large range of wave and sediment parameters: $0.95\ \mathrm{s} \leq T \leq 2.2\ \mathrm{s}$, $0.045\ \mathrm{m} \leq H \leq 0.099\ \mathrm{m}$, $111\ \mu\mathrm{m} \leq d_{50} \leq 375\ \mu\mathrm{m}$, where T and H are the wave period and height, respectively, and d_{50} the median grain size. For each test, the bed was initially flat and covered by a 25 mm sand layer. In spite of the care taken to flatten the bottom, some defects of flatness are observed. The maximum amplitude of perturbations is approximately 2 mm. The bed deformation was measured from the first excitation cycles with an optical method, detailed in [15]. The spatial resolution in the horizontal and vertical directions was 0.5 mm/pixel. The dimensions of the processed field were 5.46 m long and 0.325 m width. The ripples wavelengths at the equilibrium state were in the range $28.4\ \mathrm{mm} \leq \lambda \leq 77\ \mathrm{mm}$ for present tests. Characteristics of ripples were obtained using the one-dimensional (1D) -Hilbert transform. A great advantage of this technique is that in each patch the amplitude and phase of ripples may be determined.

Two distinct modes of ripple patterns formation are observed. In the first mode, any perturbation on the bottom is enough to trigger ripple formation and ripples form uniformly on the whole bed. In the second mode, patterns form from isolated rippled zones (described as patches by Faraci and Foti [16]). For present tests, patches appeared in zones where the characteristic amplitude of disturbances was greater or equal to the critical value of 2 mm. Two nondimensional parameters were used to characterize the regime of pattern formation: the Reynolds number Re and the Froude number Fr. These parameters are defined as follows:

*Corresponding author. francois.marin@univ-lehavre.fr

 ©2010 The American Physical Society

PROOF COPY [ERJ1041] 168009PRE

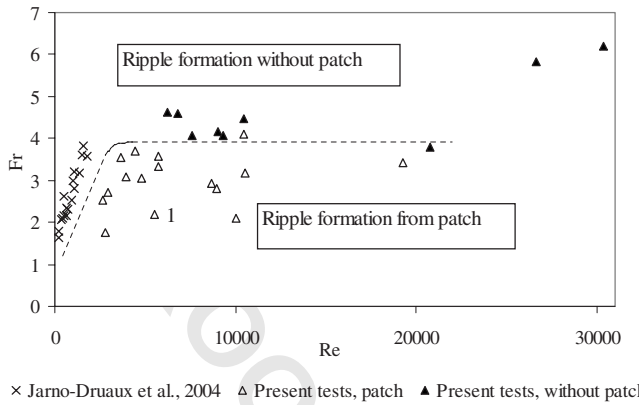

FIG. 1. Delineation of the two observed modes of ripple formation in the (Re,Fr) plane, indicating the boundary (dashed line) between the modes with and without patch (the test for which Re =5512 and Fr=2.2 is identified with the label 1).

Re$=U_\infty b/\nu$, Fr$=U_\infty/\sqrt{(s-1)gd_{50}}$, where b and U_∞ are the fluid particle semiexcursion and the fluid velocity amplitude at the edge of the bed boundary layer, respectively, s is the relative density of sediment, g the acceleration due to gravity, and ν the water kinematic viscosity. The delineation of the two observed modes of ripple formation in the (Re,Fr) plane is presented in Fig. 1. The data of Jarno-Druaux *et al.* [17] obtained in the same wave flume with lightweight grains of relative density 1.35 and median grain diameter 170 μm are also shown in this figure. Present tests show that for fixed values of Re, there is a critical value Fr$_{cr}$ of the Froude number below which ripples form from localized sites; for Fr$>$Fr$_{cr}$, no "patch" is observed. The critical Froude number becomes independent of the Reynolds number for Re >5000. This suggests that for Fr$_{cr}$=Fr$_{cr_max}\approx 3.9$, the sediments move all over the bottom with a very low resistance to motion for every hydrodynamic conditions and ripples can form everywhere on the bottom. When Fr$<$Fr$_{cr_max}$, the inertial effects become more important for increasing values of Re (keeping constant the value of Fr), and the bed local perturbations lead to patches formation. The critical value Fr$_{cr}$ grows with Re when Fr$<$Fr$_{cr_max}$. This may result from a decrease of the gravity effects in comparison with the inertial effects acting on the grains for increasing values of Fr for a given value of Re (<5000), leading to a higher mobility of the grains and preventing patch formation.

In order to study the front propagation, we focus on a test for which a slow dynamics of pattern formation from amplitude defects is observed. We have Re=5512 and Fr=2.2 for this test, and the mean ripple wavelength is $\lambda=42$ mm at the equilibrium state. An example of bed image in gray levels is given in Fig. 2 for $n=800$ excitation cycles where three main patches are clearly identified (P1 to P3). The temporal evolution of the bottom elevation is plotted as a function of the

FIG. 2. Example of bed image in gray levels for n =800 cycles (Re=5512, Fr=2.2). P1 to P3 refer to the three processed patches.

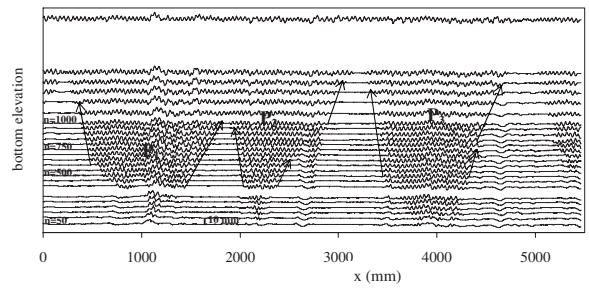

FIG. 3. Bottom elevation as a function of the x-longitudinal position and number of excitation cycles (Re=5512, Fr=2.2). The arrows show the ripple front positions detected for the three patches P1, P2, and P3.

x-longitudinal position in Fig. 3, for $y=0.20$ m where the y axis refers to the cross-section direction. The origin of the x axis is situated at 2.3 m from the wave paddle, increasing values of x corresponding to shorter distances from the absorbing beach. The time step is equal to 50 cycles for the first 1000 cycles, and afterward to 100 cycles. Isolated systems of propagating ripples can be observed during more than 1000 cycles before the invasion of the whole bottom. The estimation of front velocities can then be performed on a long time for the three observed patches. The bottom elevation signal $\eta(x,t)$ of each patch is cut into two parts in order to process the two fronts separately. The Fourier spectra of signals are then calculated and harmonics are filtered. After this filtering process, we get $\eta(x,t)=\eta_m(x,t)\cos[kx+\varphi(x,t)]$, where $\eta_m(x,t)$ is for the slow varying amplitude, $\varphi(x,t)$ is the slow varying phase of the bottom profile, and k is the bottom wave number.

Using the Hilbert transform,

$$\hat{\eta}(x,t)=\frac{1}{\pi}PV\left[\int_{-\infty}^{+\infty}\frac{\eta(x,t)}{x-\chi}d\chi\right]=\eta_m(x,t)\sin[kx+\varphi(x,t)] \quad (1)$$

where PV denotes principal value, it is possible to determine the phase and amplitude of sand ripples on the flume bottom and compare with the theoretical predictions. We can consider the bottom profile as the real part of a complex function $\eta(x,t)=\mathrm{Re}\{A(x,t)\exp[i(kx)]\}$ with $A(x,t)=|A(x,t)|e^{i\varphi(x,t)}$ and where

$$|A(x,t)|=a=\sqrt{\eta^2(x,t)+\hat{\eta}^2(x,t)},\quad \varphi(x,t)=\arctan\left(\frac{\hat{\eta}}{\eta}\right)-kx. \quad (2)$$

We extract the module of the complex amplitude a and the phase $\varphi(x,t)$ from the signals. An example of the spatial dependence for $a(x)$ and $\varphi(x)$ is shown in Fig. 4. It is important to emphasize that large changes of phase occur at wave front. The wave front is localized in the region where a transition from a low amplitude to a high (nearly constant) value is detected. We have chosen the following criterion to determine the front position: the front is situated in the region where the value of the amplitude is equal to 15% of the maximum value for the patch. The ripple fronts are presented in Fig. 3. They propagate linearly with time, and a good coefficient of regression (in the range 0.70–0.98) is obtained. The up-flow (v_{p-}; propagation in the direction opposite to the

PROOF COPY [ERJ1041] 168009PRE

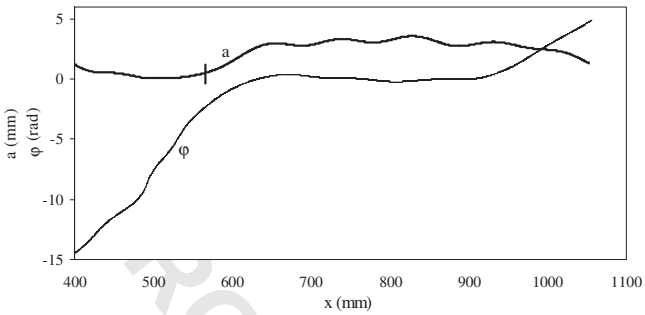

FIG. 4. Example of spatial distribution for the amplitude (bold line) and phase (thin line) of sand ripples for a front propagating upward (Patch P1, $t=550$ wave excitation cycles). The segment crossing the bold line delineates the border between the flat bottom and the ripple patch according to the criterion of threshold amplitude.

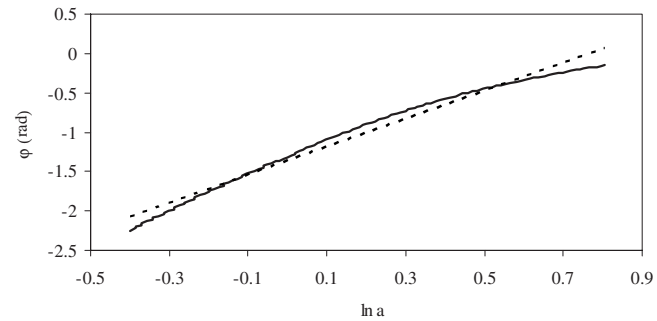

FIG. 5. Dependence of the wave phase φ on the logarithm of wave amplitude $\ln a$ for 462 mm$<x<$520 mm (bold curve) with its best linear fit approximation ($\varphi=1.82\ \ln a-1.52$; square of the correlation coefficient $R^2=0.96$; dashed line); $t=700$ wave excitation cycles.

surface waves propagation) and down-flow (v_{p+}; propagation in the same direction as the surface waves) front velocities of the patches are given in Table I. The results show that the fronts propagating in the direction of surface wave propagation have greater velocities than the fronts propagating in the opposite direction ($|v_{p+}|>|v_{p-}|$).

III. DISCUSSION OF RESULTS

According to the present experimental results, the front propagation may be considered as an envelope wave, and we have found the amplitude and phase of this envelope. Let us compare the experimental results with the solution of an equation describing the envelope amplitude, the complex Ginzburg-Landau equation (GLE) which is widely used to investigate pattern dynamics [18]. Present experiments show us that there is a threshold value of the initial bed perturbations in the front propagation regime: perturbations with an amplitude less than a critical value decay with time, whereas perturbations with an amplitude greater than the critical value grow. To take this effect into account, it is necessary to keep the nonlinear terms proportional to the third and fifth degrees of amplitude in the GLE (quintic version of GLE) [10]. The cubic version of the GLE is able to describe the linear instability of infinitely small perturbations and the nonlinear amplitude saturation. The simplest model to describe the front propagation in our system is the following:

$$\frac{\partial A}{\partial t}=(1+ic_1)\frac{\partial^2 A}{\partial x^2}+\varepsilon A+(1+ic_3)|A|^2A-(1-ic_5)|A|^4A, \quad (3)$$

where A is the complex amplitude of sand ripples, ε the super criticality ($\varepsilon<0$ in our case), and c_1,c_3,c_5 are real coefficients for dispersion (c_1), cubic nonlinearity (c_3), and quintic nonlinearity (c_5). The analytical solution of Eq. (3) has the following form [19]: $A=e^{-i\Omega t}a(\xi)e^{i\phi(\xi)}$, $\xi=x\mp Vt$ where V is the front velocity and Ω the frequency of sand ripples. The amplitude and phase obey the following differential equations (anzatz): $\partial a/\partial\xi=K_{L\mp}a(1-a^2(\xi)/a_N^2)$, $\partial\phi/\partial\xi=q_L+(q_N-q_L)a^2(\xi)/a_N^2$. For propagating fronts, the solution has the following form:

$$a=a_N e^{K_{L\mp}\xi}/\sqrt{1+e^{2K_{L\mp}\xi}}. \quad (4)$$

The amplitude grows exponentially from an infinitely small value to a constant value a_N. The six constants $K_{L\mp}$, q_L, q_N, Ω, V, a_N are determined by inserting the ansatz into Eq. (3) [10]. The sign "+" corresponds to a front which propagates in the positive direction (direction of surface waves propagation), $K_{L+}<0$, $a(x=-\infty,\ t=0)=a_N$, $a(x=+\infty,\ t=0)=0$, and the sign "−" corresponds to a front propagating in the opposite direction: $K_{L-}>0$, $a(x=-\infty,\ t=0)=0$, $a(x=+\infty,\ t=0)=a_N$. It should be noted that for regions where $a=a_N$, we have $\phi=q_N(x\mp Vt)$, and for $a\ll a_N$, $\phi\cong q_L(x\mp Vt)$. The profile of the sandy bottom may be written as $\eta(x,t)=\mathrm{Re}[A(x,t)\exp(ikx)]=a(x\mp Vt)\cos(\Omega t-q_{N,L}(x\mp Vt)-kx)$. This means that q_L and q_N may be considered as infinitesimal and finite amplitude additional terms for the wave number of sand ripples, respectively. Using the a_N^2 expression from the first equation of ansatz, we find a correlation between the phase and amplitude derivatives: $\partial\phi/\partial\xi=q_N-[(q_N-q_L)\partial a/\partial\xi]/aK_{L\pm}$, and after integration we get

$$\phi=q_N\xi-[(q_N-q_L)/K_{L\mp}]\ln a. \quad (5)$$

Excluding a linear growth of the phase with space for a given instant, we are able to present a local correlation between the wave amplitude $a(x)$ and the wave phase $\varphi(x)$: $\varphi(x)=(q_L-q_N)\ln a/K_{L\pm}$. Such correlation really occurs for the wave front in sand ripples. Figure 5 shows an example of the variation of the phase φ with the amplitude a. Using the best linear fit approximation (dashed line in Fig. 5), we determined the coefficient $\kappa_\pm=(q_L-q_N)/K_{L\pm}$. The results are different for the fronts propagating in the direction of surface waves and in the opposite direction. The values of the coefficient $\kappa_\pm$ are estimated for both fronts of Patch 1, for different numbers of excitation cycles; these values are given in

TABLE I. Up-flow and down-flow patch velocities for the three patches P1, P2, and P3 (Re=5512, Fr=2.2).

Patch	Up-flow patch velocity v_{p-} (mm s^{-1})	Down-flow patch velocity v_{p+} (mm s^{-1})
1	−0.23	0.62
2	−0.19	0.64(400$<n<$650); 0.43(1000$<n<$1400)
3	−0.16	0.37(500$<n<$800); 0.52(900$<n<$1400)

PROOF COPY [ERJ1041] 168009PRE

PROOF COPY [ERJ1041] 168009PRE

Table II. It can be noted that the linear dependence between the phase φ and $\ln a$ is obtained with lower values of the regression coefficient for fronts propagating in the direction of surface waves (except when $t=950$ excitation cycles). In this case, for some instants, no estimation of κ_+ could be proposed. The fronts propagating in the direction of surface waves are then not as regular as the fronts propagating in the opposite direction. We were able to estimate the coefficient $K_{L\pm}$: the solution (4) shows us that this exponent may approximate the amplitude growth on the wave front. Using an exponential approximation of experimental data, we have found different coefficients for the fronts: the averaged value for K_{L+} was $K_{L+}=-0.047$ mm^{-1}, and for the front propagating in the opposite direction, $K_{L-}=0.03$ mm^{-1}. The front propagating in the direction of surface waves is "steeper" than the front propagating in the opposite direction. We have estimated the changes in wave number due to the finite amplitude of sand ripples: $q_L-q_N\approx 0.039$ mm^{-1} for waves co-directed with the surface waves, and $q_L-q_N\approx 0.025$ mm^{-1} for waves propagating in the opposite direction. In both cases, the finite amplitude leads to a decrease in wave number $k+q_N$ in comparison with the linear wave number $k+q_L$, but this effect is larger for the front propagating in the direction of surface waves.

The differences between the characteristics of the fronts propagating in the same direction as the surface waves and in the opposite direction may be due to the drift induced by surface waves. It is well known [20] that in the bed boundary layer above a flat bed, induced flows lead to mass transport in the direction of waves propagation. Above sand ripples, the momentum transfer and suspended sediment dynamics are dominated by the formation and shedding at flow reversal of lee wake vortices [21]. Present data involve weakly asymmetrical waves ($B<0.1$ where $B=3bk_{sw}/4\sinh^2(k_{sw}d_*)$ and k_{sw} is the surface wave number). Using a one-dimensional vertical (1DV) two-layer model where vortex shedding is represented in the lower layer by a time-varying eddy viscosity, Davies and Thorne [21] have shown that the near-bed sand transport is in the direction of surface waves propagation for weakly asymmetrical waves. Such transport of sand increases the front velocity v_{p+} and decreases the velocity v_{p-}.

TABLE II. Values of the inclination coefficient for the upstream and downstream fronts and different numbers of excitation cycles (Patch P1). The linear regression coefficients are given in parentheses.

Number of excitation cycles	$\kappa_-=\frac{q_L-q_N}{K_{L-}}$	$\kappa_+=\frac{q_L-q_N}{K_{L+}}$
550	+1.30(R^2=0.99)	
600	+0.33(R^2=0.99)	
650	+0.45(R^2=0.99)	−1.20(R^2=0.95)
700	+1.80(R^2=0.97)	
750	+0.66(R^2=0.99)	−0.12(R^2=0.75)
800	+1.80(R^2=0.99)	−0.49(R^2=0.81)
850	+0.60(R^2=0.99)	−0.51(R^2=0.85)
900	+0.31(R^2=0.94)	−2.30(R^2=0.93)
950	+0.28(R^2=0.87)	−0.33(R^2=0.98)

IV. CONCLUSIONS

We have shown that depending on the values of the control parameters (Froude and Reynolds numbers), sand ripples on the bottom may arise as a result of two types of bifurcation: spatially homogeneous growth of small perturbations, and appearance of patches. In the last case, wave front propagation occurs. Using the Hilbert transform, we measured the amplitude and phase of ripple waves, and we have found coincidences between the experimental characteristics of propagating fronts and the analytical solution of van Saarloos and Hohenberg [19]. Such coincidences allowed us to find a correlation between the sand ripples amplitude and wave number, and conclude that there exists an effect of wave number decrease due to the finite amplitude of sand ripples. Our measurements agree with the measurements of other researchers (see, for example, [16]): the spatial period of sand ripples increases with increasing ripples amplitude. We have found that the propagating front characteristics depend on the direction of surface waves which generate ripples. If the front propagates in the direction of surface waves, it has a larger celerity, is steeper and more irregular than the front which propagates in the opposite direction. In our opinion such differences are caused by the mean flow induced by surface waves near the bottom.

[1] H. Ayrton, Proc. R. Soc. London, Ser. A **84**, 285 (1910).
[2] R. A. Bagnold, Proc. R. Soc. London, Ser. A **187**, 1 (1946).
[3] P. Blondeaux, J. Fluid Mech. **218**, 1 (1990).
[4] E. Foti and P. Blondeaux, Coastal Eng. **25**, 227 (1995).
[5] V. Marieu *et al.*, J. Geophys. Res. **113**, C09007 (2008).
[6] K. H. Andersen *et al.*, Phys. Rev. E **63**, 066308 (2001).
[7] E. K. O. Hellén and J. Krug, Phys. Rev. E **66**, 011304 (2002).
[8] T. Schnipper *et al.*, Phys. Rev. E **78**, 047301 (2008).
[9] J. L. Hansen *et al.*, Nature (London) **410**, 324 (2001).
[10] W. van Saarloos, Phys. Rep. **386**, 29 (2003).
[11] J. Fineberg and V. Steinberg, Phys. Rev. Lett. **58**, 1332 (1987).
[12] J. Fineberg *et al.*, Phys. Rev. A **41**, 5743 (1990).
[13] M. Fermigier *et al.*, J. Fluid Mech. **236**, 349 (1992).
[14] Y. Goda, *Random Seas and Design of Marine Structures* (World Scientific, Singapore, 2000).
[15] F. Marin and A. B. Ezersky, Eur. J. Mech. B/Fluids **27**, 251 (2008).
[16] C. Faraci and E. Foti, Phys. Fluids **13**, 1624 (2001).
[17] A. Jarno-Druaux *et al.*, Eur. J. Mech. B/Fluids **23**, 695 (2004).
[18] I. S. Aranson and L. Kramer, Rev. Mod. Phys. **74**, 99 (2002).
[19] W. van Saarloos and P. C. Hohenberg, Phys. Rev. Lett. **64**, 749 (1990).
[20] M. S. Longuet-Higgins, Philos. Trans. R. Soc. London, Ser. A **245**, 535 (1953).
[21] A. G. Davies and P. D. Thorne, J. Geophys. Res. **110**, C05017 (2005).

PROOF COPY [ERJ1041] 168009PRE